

# Flexible Multilevel Resistive Memory with Controlled Charge Trap B- and N-Doped Carbon Nanotubes

Sun Kak Hwang,<sup>†</sup> Ju Min Lee,<sup>†</sup> Seungjun Kim,<sup>†</sup> Ji Sun Park,<sup>†</sup> Hyung Il Park,<sup>†</sup> Chi Won Ahn,<sup>‡</sup> Keon Jae Lee,<sup>†</sup> Takhee Lee,<sup>§</sup> and Sang Ouk Kim<sup>\*†</sup>

<sup>†</sup>Department of Materials Science and Engineering, KAIST, Daejeon 305-701, Republic of Korea

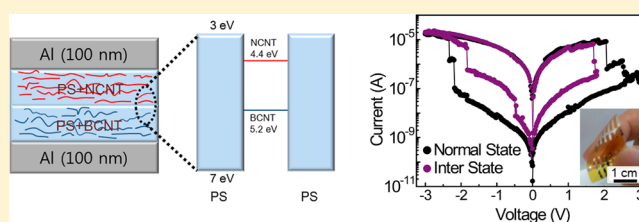
<sup>‡</sup>National Nanofab Center (NNFC), Daejeon 305-701, Republic of Korea

<sup>§</sup>Department of Physics and Astronomy, Seoul National University, Gwanak-gu, Seoul 151-742, Republic of Korea

## Supporting Information

**ABSTRACT:** B- and N-doped carbon nanotubes (CNTs) with controlled workfunctions were successfully employed as charge trap materials for solution processable, mechanically flexible, multilevel switching resistive memory. B- and N-doping systematically controlled the charge trap level and dispersibility of CNTs in polystyrene matrix. Consequently, doped CNT device demonstrated greatly enhanced nonvolatile memory performance (ON–OFF ratio  $>10^2$ , endurance cycle  $>10^2$ , retention time  $>10^5$ ) compared to undoped CNT device. More significantly, the device employing both B- and N-doped CNTs with different charge trap levels exhibited multilevel resistive switching with a discrete and stable intermediate state. Charge trapping materials with different energy levels offer a novel design scheme for solution processable multilevel memory.

**KEYWORDS:** Resistive memory, flexible memory, multilevel memory, carbon nanotube, charge trap



Resistive memory exploits the electric field responsive resistive switching of materials as an information write/erase principle for nonvolatile data storage.<sup>1–4</sup> To date, various metal oxides,<sup>5,6</sup> organic molecules,<sup>7</sup> polymers,<sup>8–13</sup> graphene oxide,<sup>14</sup> and nanocomposites<sup>15</sup> have exhibited resistive switching behaviors potentially useful for nonvolatile memory devices, including our recently introduced flexible resistive random access memory (RRAM).<sup>16</sup> Among various resistive memory devices, the nanocomposite resistive memory comprises charge trapping conductive materials, such as metal nanoparticles,<sup>17,18</sup> fullerene,<sup>19</sup> or carbon nanotubes (CNTs),<sup>20,21</sup> dispersed in a polymer matrix. The synergistic combination of the polymer matrix with facile processability and the nanomaterials with robust electrical properties provides numerous advantages, such as facile solution processing, genuine mechanical flexibility, and the tunability of resistive switching with material composition. For the successful fabrication of reliable nanocomposite resistive memory, uniform dispersion of charge trapping materials in a polymer matrix is crucial. Nevertheless, the currently available surface modification methods to promote the dispersibility may cause the undesired modification of charge trapping properties. Widely used organic surface modifiers cause a significant energy barrier between charge trapping materials and the polymer matrix.<sup>22,23</sup> The harsh chemical treatment frequently employed for surface functionalization severely deteriorates the charge trapping capacity and long-term stability.<sup>24</sup>

Increasing demands for high density data storage have triggered a particular research attention to multilevel switching

resistive memory. The multilevel tunability of resistivity offers a unique opportunity to store more than 2-bits in a single cell, thereby achieving a high density memory with minimized downscaling. A stable operation of multilevel switching generally requires a long retention time and a large ON–OFF ratio of different resistive states.<sup>25,26</sup> Meanwhile, the nanocomposite resistive memory has never demonstrated such multilevel switching characteristics thus far. Without a robust strategy to control the energy levels of charge trapping materials, discrete and stable multilevel resistivity states could hardly have been attained.

In this work, we present mechanically flexible, multilevel switching resistive memory fabricated from the facile solution casting of polystyrene (PS)/chemically doped multiwalled CNT-nanocomposites. It is generally considered that the workfunction of CNTs, destined by the inert graphitic chemical structure, is difficult to modify.<sup>27</sup> Nevertheless, the tunability of the workfunction may provide an effective pathway to stabilize multiple resistivity levels. We succeeded in the systematic tuning of the workfunction (and thus charge trapping behavior) of CNTs via substitutional doping with boron (B) and nitrogen (N) atoms.<sup>28–34</sup> Electron rich N-doping effectively and permanently lowered the workfunction (shallow charge trap) while electron deficient B-doping significantly increased it (deep charge trap). In addition, the substitutional doping of

**Received:** November 16, 2011

**Revised:** March 16, 2012

**Published:** April 20, 2012

heteroatoms in the graphitic plane of CNTs remarkably enhanced the dispersibility of CNTs in the polymer matrix with no surface modifier. These advantages make it possible to control the electrical switching characteristics of the doped CNT composite devices with workfunction or concentration of doped CNTs. As a consequence, the fabricated devices consisting of metal/CNT nanocomposites/metal multilayers demonstrated the rewritable nonvolatile memory characteristics with mechanical deformability and long-term stability in an ambient condition. More significantly, the tunability of CNT workfunction enabled the unprecedented operation of multi-level resistive switching with discrete resistivity states.

A resistive memory device consisting of Al-electrode/CNT-nanocomposites/Al-electrode deposited on flexible polyimide is schematically illustrated in Figure 1(a). Scanning electron

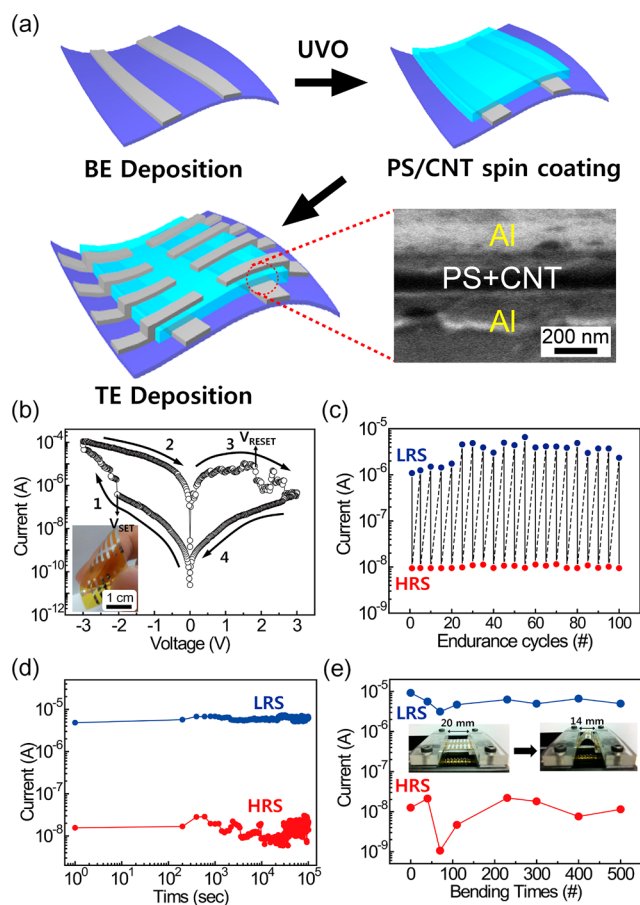


**Figure 1.** (a) Schematic and SEM image of the CNT nanocomposite memory device. (b)  $I$ - $V$  characteristics of the Al/PS + BCNT (1.5 wt %)/Al devices. The inset is a photograph exhibiting the flexibility. (c) Endurance cycles and (d) retention characteristics of the devices under  $-1$  V read voltage. (e) The ON and OFF current characteristics of the flexible device according to bending times. The insets show photographs of two repeated bending states.

microscopy (SEM) shows the cross-sectional view. The B- and N-doping of CNTs were performed by thermal treatment under an Ar/NH<sub>3</sub> stream with and without vaporized B<sub>2</sub>O<sub>3</sub>, respectively.<sup>28</sup> The top electrode (TE) and bottom electrode (BE) Al were prepared by thermal evaporation with shadow masks. We note that the BE Al bottom electrode was treated with UV ozone (UVO) before spin-casting CNT-nanocomposite layer. XPS characterization revealed that stable

native oxide (AlO<sub>x</sub>) layer was formed at the surface of BE (Supporting Information, Figure S1) after UVO treatment. This AlO<sub>x</sub> layer strongly influenced the reproducible switching of resistive memory, as described below.<sup>4,14</sup> The 100 nm thick PS/CNT nanocomposite layer was directly spin-cast from organic solution onto BE Al. The precursor solution was prepared by the simple dissolution of the predetermined amounts of PS and CNTs in dichlorobenzene with no surface modifier.

Figure 1b shows the current-voltage ( $I$ - $V$ ) characteristics of the device with 1.5 wt % BCNT. The arrows indicate the voltage sweeping direction. In the first voltage sweep from 0 to  $-3$  V, the current increased gradually in the beginning but increased more rapidly above a SET voltage ( $V_{\text{SET}}$ ) of  $-2.0$  V. This corresponds to the transition from high-resistance state (HRS) to low-resistance state (LRS). In the following sweep from  $-3$  to 0 V, the device sustained the LRS. Meanwhile, the current abruptly decreased during the sweep from 0 to  $+3$  V, which is the transition from LRS to HRS at a higher RESET voltage ( $V_{\text{RESET}}$ ). In this RESET sweep, the AlO<sub>x</sub> layer at BE surface blocked the electron injection from BE. Consequently, the electrons trapped in CNT could be released into TE without retrapping. The SET did not occur at a positive voltage on TE electrode due to the AlO<sub>x</sub> layer on BE electrode (Supporting Information, Figure S2). It is noteworthy that this significant role of the AlO<sub>x</sub> blocking layer could be confirmed by comparing the device properties with a bare Au electrode (without AlO<sub>x</sub> layer) and with AlO<sub>x</sub> layer, whose thickness was tunable by UVO treatment. As anticipated, the device showed breakdown without the AlO<sub>x</sub> layer and the thickness of the AlO<sub>x</sub> layer significantly influenced the device performance, such as ON/OFF current (Supporting Information, Figure S3). The device maintained the HRS in the final sweep from  $+3$  to 0 V. The rewritable cycles (write-read-erase-read) could be repeated over 100 times (Figure 1c). The flexible devices exhibited stable retention times longer than 10<sup>5</sup> s and showed stable resistive memory characteristics, even after being bent severely more than 500 times (Figure 1d,e). The device also exhibited excellent air stability, which could be confirmed by the device characterization after prolonged exposure to ambient conditions. The  $I$ - $V$  characteristics of the Al/BCNT-nanocomposites/Al device did not show a noticeable change after 7 and 15 days of exposure to air (Supporting Information, Figure S4). Such high air stability ensured the reliable operation of flexible resistive memory fabricated on the flexible polyimide substrate without particular encapsulation.

Figure 2a shows the  $I$ - $V$  characteristics of the devices with pure PS, PS/undoped CNT, PS/N-doped CNT (denoted as NCNT), and PS/BCNT nanocomposite layers. The  $I$ - $V$  characteristics of an Al/PS/Al device showed a typical dielectric curve without hysteresis.<sup>35</sup> In contrast, the nanocomposite devices with CNTs exhibited the hysteresis caused by rewritable organic resistive memory characteristics. Figure 2b compares the current values for the HRS and LRS of the nanocomposite devices measured under a constant  $-1$  V read voltage. The CNT composition was 1.5 wt % for all devices. The ON-OFF ratios of the devices with BCNTs ( $\sim 4 \times 10^2$ ) and NCNTs ( $\sim 10^2$ ) were approximately one order higher than that of the device with undoped CNTs ( $\sim 10$ ). While the device with undoped CNTs showed unstable retention that gradually transitioned from HRS to LRS with severe fluctuation, the devices with BCNTs and NCNTs sustained consistent current values of LRS and HRS for longer than 10<sup>3</sup> s. The high retention

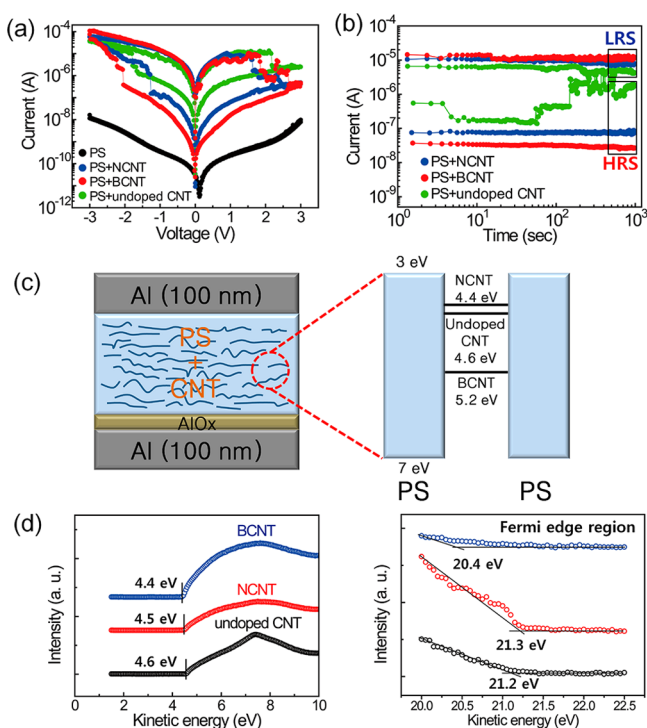


**Figure 2.** (a)  $I$ - $V$  and (b) retention characteristics of the resistive memory devices. (c) Energy band diagram of the device. (d) Workfunction measurement of undoped CNT, BCNT, and NCNT by UPS.

stability of doped CNT is attributed to the enhanced dispersibility of CNTs in the PS matrix, as discussed below.

The reflective optical microscopy images were obtained to compare the morphology of nanocomposite memory devices (Supporting Information, Figure S5). Dense dark CNT aggregates appeared in the devices with undoped CNTs, whereas CNT aggregates were rarely observed in the devices with BCNTs and NCNTs. It is well-known that raw CNTs are hardly dispersed in a polymer matrix without surface modifier due to the low surface energy of CNTs and the strong van der Waals interaction among CNTs. The aggregation of CNTs may significantly reduce the charge trap density in the PS matrix and induce the localization of an electric field around CNTs, which can significantly degrade the device performance. In contrast, the BCNTs and NCNTs accompany local positive and negative charges at the doped B and N heteroatoms, respectively. The local charges induce net repulsion among neighboring CNTs and enhance the surface energy of CNTs. Consequently, BCNTs and NCNTs showed remarkably improved dispersion in organic solvent or polymer media without any surface modifier.<sup>28</sup>

The resistive switching mechanism of our nanocomposite devices was investigated by  $I$ - $V$  measurements (Supporting Information, Figure S6). The  $I$ - $V$  curve was well fitted to trap control space charge limited current (SCLC) conduction mechanism.<sup>36</sup> The trap-controlled SCLC consists of four regimes: an ohmic regime ( $I \propto V$ ), a trap-limited SCLC regime ( $I \propto V^2$ ), a trap-filled limited regime ( $I \propto V^\alpha$ ,  $\alpha > 2$ ), and a trap-free SCLC regime ( $I \propto V^2$ ). The trap-controlled SCLC describes the charge conduction via charge trap and detrapping. The consistency with this models confirms that the switching mechanism of our CNT nanocomposite memory

follows the charge storage mechanism by trapping and detrapping.<sup>37,38</sup>

As presented in Figure 2a, the OFF-current of the NCNT device ( $1.1 \times 10^{-7}$  A) measured at  $-1$  V bias was approximately three times higher than that of the BCNT device ( $3.7 \times 10^{-8}$  A). In the charge-trapping resistive memory, the device characteristics can be closely related to the energy level of charge trapping materials. Figure 2c showed the energy band diagrams of our nanocomposite devices. PS is a wide band gap insulator with the highest occupied molecular orbital (HOMO) level of 7.0 eV and the lowest unoccupied molecular orbital (LUMO) level of 3.0 eV.<sup>39</sup> The workfunction of the Al electrode is known to be 4.2 eV. The workfunction of the doped CNT was measured by ultraviolet photoemission spectroscopy (UPS) employing a He I (21.2 eV) photon source. The workfunction was taken from the energy level difference between the inelastic cut off and the Fermi edge (Figure 2d). While the workfunction of undoped CNT was 4.6 eV, that of BCNT was enhanced up to 5.2 eV, as electron deficient B-doping effectively lowered the  $\pi$ -electron density. In contrast, the workfunction of NCNT slightly decreased down to 4.4 eV due to the additional  $\pi$ -electrons from electron-rich N atoms. As described in Figure 2c, the energy level difference between the workfunction of NCNTs and the LUMO of PS was 1.4 eV while that with BCNTs was 2.2 eV. If the energy level difference is large, electrons can be deeply trapped in the CNTs surrounded by PS. As a consequence, the BCNT device could release electrons from traps at a higher voltage (higher  $V_{\text{RESET}}$ ) and show a lower OFF-current value compared with the NCNT device. This result demonstrates that the workfunction tunability of charge trapping CNT is an effective route to control the resistive switching behavior. The energy level of charge trapping CNTs also influenced the  $V_{\text{SET}}$  value. The  $V_{\text{SET}}$  of the NCNT device ( $-1.2$  V) was  $\sim 0.8$  V lower than that of the BCNT device ( $-2.0$  V) (Figure 2a). This is attributed to the energy level difference between the anode and neighboring CNT trap sites.<sup>40</sup> The energy difference between NCNT and Al was 0.2 eV while that for BCNT was 1.0 eV. A low energy level difference may cause direct tunneling electrons from the CNT trap to a nearby anode with a low potential barrier. The distribution data of switching parameters for BCNT and NCNT devices showed by a box-whisker plot obtained from  $I$ - $V$  curves of 30 unit cells (Supporting Information, Figure S7).

We investigated and compared the resistive memory characteristics with various CNT compositions (0.5–3.0 wt %). Owing to the fine dispersibility, all the devices with NCNTs and BCNTs exhibited reliable rewritable organic resistive memory characteristics (Supporting Information, Figures S8). The ON- and OFF-current values increased with the composition of doped CNTs while the  $V_{\text{SET}}$  decreased (Supporting Information, Figure S9). The current value was proportional to the charge trap density given by the CNT composition. Meanwhile, the average separation between neighboring CNTs should decrease with CNT composition (Supporting Information, Figure S10). The electrons captured in a CNT could readily transfer to the neighboring CNTs (low  $V_{\text{SET}}$ ) if the separation between neighboring CNTs is close. We note that the ON-OFF ratio maintained almost the same value with BCNT composition and suddenly decreased at the 3.0 wt % (Supporting Information, Figure S9 left). Since the increase of charge trap density was compensated by the decrease in the average separation between neighboring CNTs (lower  $V_{\text{SET}}$ ), the ON-OFF ratio maintained the almost same value up to 2.5

wt %. The sudden decrease at 3.0 wt % is attributed to the initiation of the partial percolation of CNTs. This variation of resistive switching behavior with CNT composition also supports that well-dispersed doped CNTs indeed played the role of charge trap in the PS matrix. In the retention characteristics, all the devices with different CNT compositions sustained the initial ON- and OFF-current values for more than  $10^3$  s under a constant  $-1$  V read voltage (Supporting Information, Figure S11).

The workfunction tunability of CNT by chemical doping could be successfully exploited for mechanically flexible multilevel switching resistive memory. The devices consisting of the quadruple layers of Al/BCNT–nanocomposites/NCNT–nanocomposites/Al were prepared on polyimide substrates (Figure 3a). The first BCNT–nanocomposite layer was spin-

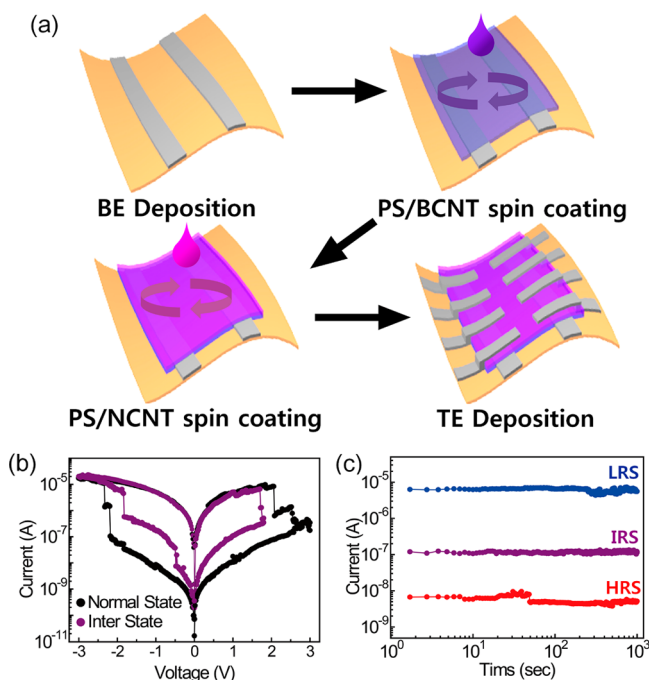


**Figure 3.** (a) A schematic illustration of the fabrication process of the multistate resistive memory device. (b)  $I$ – $V$  and (c) retention characteristics of multistate devices.

cast and subsequently cross-linked by UV to prevent the intermixing with the second NCNT–nanocomposite layer during spin-casting. As presented in Figure 3b, the flexible device with a quadruple layer exhibited stable triple state memory characteristics (i.e., LRS, HRS and interstate (IRS)) unlike triple layer devices consisting of Al/BCNT or NCNT–nanocomposites/Al. The multilevel memory devices store more than 2-bits in a single cell, thereby achieving a high density memory without complex concepts such as downscaling. In the retention characteristics, the device stably sustained the initial current values of HRS, IRS, and LRS for more than  $10^3$  s under a constant  $-1$  V read voltage. In the negative bias range, the  $V_{SET}$  values for HRS and IRS were  $-2.2$  and  $-1.8$  V, respectively. The current ratios for LRS/IRS and IRS/HRS were 50 and 15, respectively.

The operation mechanism of the multilevel switching employing both BCNT- and NCNT-nanocomposites is presented in Figure 4. The IRS was stabilized by the selective electron trap in NCNTs with a shallow level. After the full

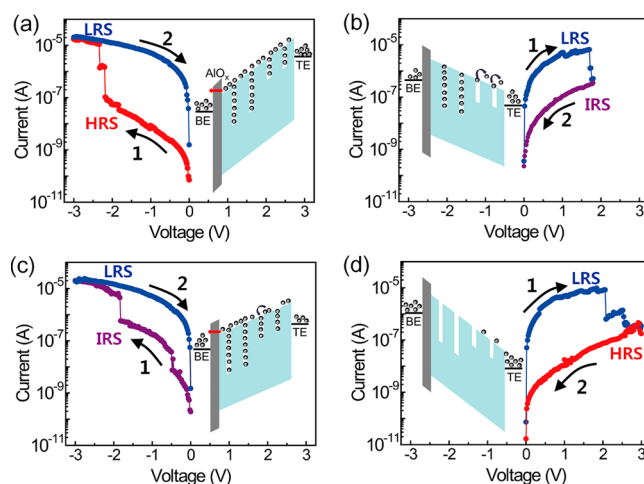


**Figure 4.** Multilevel switching mechanism of the quadruple layer device (see text for details).

electron trap during the first sweep from 0 to  $-3$  V (Figure 4a), the electrons trapped in NCNT were selectively released at a low positive voltage ( $+1.8$  V) (Figure 4b). As a result, the device transitioned from LRS to IRS and sustained the IRS ((1 to 2) in Figure 4b). The device transitioned from the IRS to the fully charged LRS when vacant NCNT traps were occupied by injected electrons again during the second sweep from 0 to  $-3$  V ((1 to 2) in Figure 4c) and sustained the LRS from  $-3$  from 0 V. At the last stage of a cycle, the device transitioned from the LRS to the HRS at  $+3$  V while all the electrons trapped in both NCNT and BCNT traps were fully released (Figure 4d). The discrete energy levels of NCNT and BCNT enabled the highly stable intermittent switching levels of resistive memory.

In summary, we have presented mechanically flexible nonvolatile resistive memory with multilevel switching behavior employing charge trap controllable BCNTs and NCNTs. The controlled workfunction and high dispersibility of substitutionally doped CNTs significantly improved the resistive memory performance of CNT nanocomposite devices. An ON–OFF ratio of larger than  $10^2$ , endurance cycles of more than  $10^2$ , and a retention time of longer than  $10^5$  s were achieved with good mechanical flexibility and long-term air stability. Furthermore, the controllable CNT workfunction enabled the unprecedented operation of multilevel resistive switching with a discrete intermediate resistivity state. The ON–OFF ratios of LRS/IRS and IRS/HRS were 50 and 15, respectively. In the retention characteristics, the device stably sustained the current of HRS, IRS, and LRS for more than  $10^3$  s under a constant  $-1$  V read voltage. Our nanocomposite device architecture with the charge trapping materials with different energy levels offers a promising and reliable design scheme for the low cost solution processing of flexible multilevel resistive memory.

## ■ ASSOCIATED CONTENT

### 📄 Supporting Information

Supporting results are available free of charge *via* the Internet at <http://pubs.acs.org>.

## ■ AUTHOR INFORMATION

### ✉ Corresponding Author

\*E-mail: [sangouk.kim@kaist.ac.kr](mailto:sangouk.kim@kaist.ac.kr). Phone:  $+82-42-350-3339$ . Fax:  $+82-42-350-3310$ .

## Notes

The authors declare no competing financial interest.

## ■ ACKNOWLEDGMENTS

This work was supported by the National Research Laboratory Program (ROA-2008-000-20057-0), Converging Research Center Program (2011K000642), and the Smart IT Convergence System Research Center (Global Frontier Project) funded by MKE and MEST of Republic of Korea.

## ■ REFERENCES

- (1) Yang, Y.; Ouyang, J.; Ma, L.; Tseng, R. J. H.; Chu, C. W. *Adv. Funct. Mater.* **2006**, *16*, 1001–1014.
- (2) Scott, J. C.; Bozano, L. D. *Adv. Mater.* **2007**, *19*, 1452–1463.
- (3) Park, Y. J.; Bae, I.-S.; Kang, S. J.; Chang, J.; Park, C. *IEEE Trans. Dielectr. Electr. Insul.* **2010**, *17*, 1135–1162.
- (4) Cho, B.; Song, S.; Ji, Y.; Kim, T. W.; Lee, T. *Adv. Funct. Mater.* **2011**, *21*, 2806–2829.
- (5) Waser, R.; Aono, M. *Nat. Mater.* **2007**, *6*, 833–840.
- (6) Kwon, D. H.; Kim, K. M.; Jang, J. H.; Jeon, J. M.; Lee, M. H.; Kim, G. H.; Li, X. S.; Park, G. S.; Lee, G. S.; Lee, B.; Han, S.; Kim, M.; Hwang, C. S. *Nat. Nanotechnol.* **2010**, *5*, 148–153.
- (7) Li, Y.; Qiu, D.; Cao, L.; Shao, C.; Pan, L.; Pu, L.; Xu, J.; Shi, Y. *Appl. Phys. Lett.* **2010**, *96*, 133303.
- (8) Fang, Y. K.; Liu, C. L.; Chen, W. C. *J. Mater. Chem.* **2011**, *21*, 4778–4786.
- (9) Hahm, S. G.; Choi, S.; Hong, S. H.; Lee, T. J.; Park, S.; Kim, D. M.; Kwon, W. S.; Kim, K.; Kim, O.; Ree, M. *Adv. Funct. Mater.* **2008**, *18*, 3276–3282.
- (10) Liu, S. J.; Lin, Z. H.; Zhao, Q.; Ma, Y.; Shi, H. F.; Yi, M. D.; Ling, Q. D.; Fan, Q. L.; Zhu, C. X.; Kang, E. T.; Huang, W. *Adv. Funct. Mater.* **2011**, *21*, 979–985.
- (11) Patil, S.; Lai, Q.; Marchioni, F.; Jung, M.; Zhu, Z.; Chen, Y.; Wudl, F. *J. Mater. Chem.* **2006**, *16*, 4160–4164.
- (12) Qixi, L.; Lei, L.; Zhiyong, L.; Stickle, W. F.; Williams, R. S.; Chen, Y. *Appl. Phys. Lett.* **2009**, *95*, 213503.
- (13) Kang, S. J.; Bae, I.-S.; Shin, Y. J.; Park, Y. J.; Huh, J.; Park, S. M.; Kim, H. C.; Park, C. *Nano Lett.* **2011**, *11*, 138–144.
- (14) Jeong, H. Y.; Kim, J. Y.; Kim, J. W.; Hwang, J. O.; Kim, J. E.; Lee, J. Y.; Yoon, T. H.; Cho, B. J.; Kim, S. O.; Ruoff, R. S.; Choi, S. Y. *Nano Lett.* **2010**, *10*, 4381–4386.
- (15) Ouyang, J.; Chu, C. W.; Szmanda, C. R.; Ma, L.; Yang, Y. *Nat. Mater.* **2004**, *3*, 918–922.
- (16) Kim, S.; Jeong, H. Y.; Kim, S. K.; Choi, S. Y.; Lee, K. J. *Nano Lett.* **2011**, *11*, 5438–5442.
- (17) Tseng, R. J.; Huang, J.; Quyang, J.; Kaner, R. B.; Yang, Y. *Nano Lett.* **2005**, *5*, 1077–1080.
- (18) White, S. I.; Vora, P. M.; Kikkawa, J. M.; Winey, K. I. *Adv. Funct. Mater.* **2011**, *21*, 233–240.
- (19) Song, S.; Cho, B.; Kim, T. W.; Ji, Y.; Jo, M.; Wang, G.; Choe, M.; Kahng, Y. H.; Hwang, H.; Lee, T. *Adv. Mater.* **2010**, *22*, 5048–5052.
- (20) Pradhan, B.; Batabyal, S. K.; Pal, A. J. *J. Phys. Chem. B* **2006**, *110*, 8274–8277.
- (21) Liu, G.; Ling, Q. D.; Teo, E. Y. H.; Zhu, C. X.; Chan, D. S. H.; Neoh, K. G.; Kang, E. T. *ACS Nano* **2009**, *3*, 1929–1937.
- (22) Ma, H.; Yip, H. L.; Huang, F. H.; Jen, A. K.-Y. *Adv. Funct. Mater.* **2010**, *20*, 1371–1388.
- (23) Yip, H. L.; Hau, S. K.; Baek, N. S.; Ma, H.; Jen, A. K.-Y. *Adv. Mater.* **2008**, *20*, 2376–2382.
- (24) Chaudhary, S.; Lu, H.; Müller, A. M.; Bardeen, C. J.; Ozkan, M. *Nano Lett.* **2007**, *7*, 1973–1979.
- (25) Park, J. G.; Nam, W. S.; Seo, S. H.; Kim, Y. G.; Oh, Y. H.; Lee, G. S.; Paik, U. G. *Nano Lett.* **2009**, *9*, 1713–1719.
- (26) Nagashima, K.; Yanagida, T.; Oka, K.; Taniguchi, T. K.; Kim, J.; Park, B. H. *Nano Lett.* **2010**, *10*, 1359–1363.
- (27) Berson, S.; Bettignies, R.; Bailly, S.; Guillerez, S.; Joussetme, B. *Adv. Funct. Mater.* **2007**, *17*, 3363–3370.
- (28) Lee, J. M.; Park, J. S.; Lee, S. H.; Kim, H.; Yoo, S.; Kim, S. O. *Adv. Mater.* **2011**, *23*, 629–633.
- (29) Lee, S. H.; Lee, D. H.; Lee, W. J.; Kim, S. O. *Adv. Funct. Mater.* **2011**, *21*, 1338–1354.
- (30) Hwang, J. O.; Park, J. S.; Choi, D. S.; Kim, J. Y.; Lee, S. H.; Lee, K. E.; Kim, Y.-H.; Song, M. H.; Yoo, S.; Kim, S. O. *ACS Nano* **2012**, *6*, 159–167.
- (31) Lee, D. H.; Lee, W. J.; Kim, S. O.; Kim, Y. -H. *Phys. Rev. Lett.* **2011**, *106*, 175502.
- (32) Park, S. J.; Hu, Y.; Hwang, J. O.; Lee, E. -S.; Casabianca, L. B.; Cai, W.; Potts, J. R.; Ha, H.-W.; Chen, S.; Oh, J. H.; Kim, S. O.; Kim, Y. -H.; Ishii, Y.; Ruoff, R. S. *Nat. Commun.* **2012**, *3*, 638.
- (33) Lee, D. H.; Lee, W. J.; Kim, S. O. *Nano Lett.* **2009**, *9*, 1427–1432.
- (34) Yun, J. M.; Kim, K. N.; Kim, J. Y.; Shin, D. O.; Lee, W. J.; Lee, S. H.; Liberman, M.; Kim, S. O. *Angew. Chem., Int. Ed.* **2012**, *124*, 936–939.
- (35) Kim, C.; Facchetti, A.; Marks, T. J. *Science* **2007**, *318*, 76–80.
- (36) Lampert, M. A.; Mark, P. *Current Injection in Solids*; Academic: New York, 1970.
- (37) Lin, H. T.; Pei, Z.; Chan, Y. J. *IEEE. Electron Device Lett.* **2007**, *28*, 569–571.
- (38) Bozano, L. D.; Kean, B. W.; Deline, V. R.; Salem, J. R.; Scott, J. C. *Appl. Phys. Lett.* **2004**, *84*, 607–609.
- (39) Duke, C. B.; Fabish, T. J. *Phys. Rev. Lett.* **1976**, *37*, 1075–1077.
- (40) Ouyang, J.; Yang, Y. *Appl. Phys. Lett.* **2010**, *96*, 063506.